CHAPTER 15

A STUDY ON MASS TRANSPORT IN BOUNDARY LAYERS IN STANDING WAVES

Hideaki Noda

Assistant Professor of Hydraulics
Disaster Prevention Research Institute
Kyoto University, Kyoto, Japan

ABSTRACT

This paper deals with the mass transport in the boundary layers developed on smooth and horizontal bottoms by standing waves in shallow water. In a theoretical approach, the basic equations of laminar boundary layers are applied to solving the oscillatory motion in the boundary layers caused by the standing waves. The mass transport velocities are derived on the basis of solutions of the second approximation which describe the flow velocity near the bottom, and the effects of convective terms involved in the basic equations are investigated.

Experimental measurements in standing waves of mass transport velocity in the bottom boundary layer were carried out using dye-streak and solid-particle methods. The experimental data are compared with the theoretical prediction.

INTRODUCTION

The depositional behaviour of sediments is an important factor in the control of shoaling in harbor basins and the maintenance of the harbor function for navigation. The considerations developed in this paper began with some of the problems of the Gumizaki Fishery Harbor being filled up by drifting sands.

It has been shown in the previous paper, presented at the Tenth Conference on Coastal Engineering, that sand bars are formed at definite locations in a harbor basin, and that the standing waves induced in the harbor basin play an important role in the formation of these bars. Lettau (Ref.1) has theoretically shown that sand bars are formed at the anti-node positions of standing waves by the deposition of suspended sediments. On the other hand, Nomitsu (Ref. 2) has described bar formation at both the node and anti-node positions of standing waves by the movement of bed loads. Hayami (Ref. 3) has also shown that the filling-up of the basin by drifting sands in Tomari Harbor can be explained by Nomitsu's theory. Nevertheless, the author's experimental results differ from his prediction: these bars are formed only at the anti-node of standing waves.

The movement of sediments is caused by the fluid motion near the bed. Therefore, the resolution of this question is necessary in order to give an adequate description of the characteristics of the oscillatory motion near the bottom due to standing waves. The mechanism of such bar formation must then be found on the basis of the above description. Therefore, an attempt has been made to study the fluid motion in the boundary layers developed on smooth bottoms in the case of standing waves in shallow water of uniform depth, especially the velocity profile and the mass transport velocity in the boundary layers.

Longuet-Higgins (Ref. 4) derived an appropriate field equation for the stream function of the mass transport, and described a general method for determining the mass transport velocity in the boundary layers. In general, it is well known that in the irrotational standing waves the mass transport velocity vanishes everywhere. However, Longuet-Higgins showed the existence of the mass transport in the boundary layers by taking into account the viscous action of the fluid, even in standing waves.

On the other hand, Iwagaki and Tuchiya (Ref. 5) described the perturbation method for determining the velocity profile in the boundary layers developed on the bottom of a wave tank by progressive waves, when they treated the problem of wave damping due to bottom friction.

In this paper, the latter method is applied to the case of standing waves. By this method, an approximate solution of non-linear, laminar boundary layer equations is applied to deriving the mass transport velocities of this layer in standing waves. The author's result for the mass transport velocity is in agreement with that predicted by Longuet-Higgins.

Experimental measurements of mass transport velocity in the boundary layer near the bottom under standing waves are then compared with theoretical results.

THEORY OF LAMINAR BOUNDARY LAYER DUE TO STANDING WAVES

For two-dimensional case, the laminar boundary layer equations on the assumption of incompressible fluid are given by:

$$\left.\begin{aligned}
&\frac{\partial u}{\partial t}+u\frac{\partial u}{\partial x}+w\frac{\partial u}{\partial z}=-\frac{1}{\rho}\frac{\partial p}{\partial x}+\nu\frac{\partial^2 u}{\partial z^2}\\
&\frac{\partial u}{\partial x}+\frac{\partial w}{\partial z}=0\\
&-\frac{1}{\rho}\frac{\partial p}{\partial x}=\frac{\partial u_\infty}{\partial t}+u_\infty\frac{\partial u_\infty}{\partial x}
\end{aligned}\right\}\qquad(1)$$

in which x is the horizontal distance from the vertical wall of one end of a wave tank, z the vertical distance from the bottom, t the time, p the pressure, ρ the density, ν the kinematic viscosity, u and w the velocity components in the boundary layer in the direction of x and z, respectively and u_∞ the velocity just outside the boundary layer due to the finite amplitude wave theory.

Selecting the wave length of standing waves L and the boundary layers thickness parameter $\delta = (\nu T/2\pi)^{1/2}$ as the representative length, and using the dimensionless quantities defined as follows:

$$\left.\begin{aligned} &u = Cu^*,\ w = \omega\delta w^*,\ p = \rho C^2 p^*,\ u_\infty = C u_\infty^* \\ &x^* = kx,\ t^* = \omega t,\ z^* = z/\delta,\ h^* = kh \end{aligned}\right\} \tag{2}$$

the non-dimensional form of Eq.(1) can be expressed by:

$$\left.\begin{aligned} &\frac{\partial u^*}{\partial t^*} + u^*\frac{\partial u^*}{\partial x^*} + w^*\frac{\partial u^*}{\partial z^*} = \frac{\partial u_\infty^*}{\partial t^*} + u_\infty^*\frac{\partial u_\infty^*}{\partial x^*} + \frac{\partial^2 u^*}{\partial z^{*2}} \\ &\frac{\partial u^*}{\partial x^*} + \frac{\partial w^*}{\partial z^*} = 0 \end{aligned}\right\} \tag{3}$$

in which T is the wave period, h the water depth, $C = L/T$, $\omega = 2\pi/T$, and $k = 2\pi/L$. The boundary conditions for Eq.(3) can be written as

$$\left.\begin{aligned} &u^* = 0 \text{ and } w^* = 0 \quad \text{at } z^* = 0, \\ &u^* = u_\infty^* \qquad\qquad\quad \text{at } z^* \to \infty . \end{aligned}\right\} \tag{4}$$

The velocity just outside the boundary layers u_∞^* on the basis of the finite amplitude wave theory is given by:

$$u_\infty^* = -\left(\frac{H}{L}\right)\frac{\pi}{\sinh h^*}\sin x^* \cos t^* - \left(\frac{H}{L}\right)^2\frac{3\pi^2}{8\sinh^4 h^*}\cos 2x^* \sin 2t^* - \cdots\cdots \tag{5}$$

for the case of standing waves, in which H is the wave height.

The solution of Eq.(3) can be obtained by the perturbation method which expresses the solution of u^* and w^*, respectively as follows:

$$\left.\begin{aligned} &u^* = \varepsilon u_1^* + \varepsilon^2 u_2^* + \cdots\cdots\cdots \\ &w^* = \varepsilon w_1^* + \varepsilon^2 w_2^* + \cdots\cdots\cdots \end{aligned}\right\} \tag{6}$$

in which a small quantity ε is equal to H/L .

From Eq.(5), the velocity just outside the boundary layers can be rewritten by:

$$u_\infty^* = \varepsilon u_{\infty 1}^* + \varepsilon^2 u_{\infty 2}^* + \cdots\cdots\cdots \tag{7}$$

in which

$$\left.\begin{aligned} u_{\infty 1}^* &= -\frac{\pi}{\sinh h^*} \sin x^* \cos t^* , \\ u_{\infty 2}^* &= -\frac{3\pi^2}{8\sinh^4 h^*} \cos 2x^* \sin 2t^* \end{aligned}\right\} \tag{8}$$

Substituting these expressions into Eq.(3) gives the differential equations of the first approximation for u_1^* and w_1^*:

$$\left.\begin{aligned} \frac{\partial u_1^*}{\partial t^*} - \frac{\partial^2 u_1^*}{\partial z^{*2}} &= \frac{\partial u_{\infty 1}^*}{\partial t^*} \\ \frac{\partial u_1^*}{\partial x^*} + \frac{\partial w_1^*}{\partial z^*} &= 0 \end{aligned}\right\} \tag{9}$$

with the boundary conditions $u_1^* = w_1^* = 0$ at $z^* = 0$ and $u_1^* = u_{\infty 1}^*$ at $z^* \to \infty$. Eq.(9) indicates the linearized theory and its solutions are given by:

$$\begin{aligned} u_1^* &= -\hat{u}_{\infty 1}^* \sin x^* \{\cos t^* - e^{-\eta^*} \cos(t^* - \eta^*)\}, \\ w_1^* &= -\hat{u}_{\infty 1}^* \cos x^* \{\sqrt{2}\,\eta^* \cos t^* + e^{-\eta^*} \cos(t^* - \eta^* - \pi/4) - \cos(t^* - \pi/4)\} \end{aligned} \tag{10}$$

in which $\eta^* = z^*/2$ and $\hat{u}_{\infty 1}^* = \pi/\sinh h^*$.

For u_2^* , the equation of the second approximation can be written by:

$$\begin{aligned} \frac{\partial u_2^*}{\partial t^*} - \frac{1}{4}\frac{\partial^2 u_2^*}{\partial \eta^{*2}} = \frac{1}{4}\hat{u}_{\infty 1}^{*2} \sin 2x^* \Big[& (1+\sqrt{2}\,\eta^*) e^{-\sqrt{2}\eta^*} \cos(2t^* - \sqrt{2}\,\eta^*) \\ & - \sqrt{2}\,\eta^* e^{-\sqrt{2}\eta^*} \sin(2t^* - \sqrt{2}\,\eta^*) \\ & - 8\,(\hat{u}_{\infty 2}^* / \hat{u}_{\infty 1}^{*2}) \cot 2x^* \cos 2t^* \Big] \\ + \frac{1}{8}\hat{u}_{\infty 1}^{*2} \sin 2x^* \Big[& 2(2 + \sqrt{2}\,\eta^*) e^{-\sqrt{2}\eta^*} \cos\sqrt{2}\,\eta^* - 2e^{-2\sqrt{2}\eta^*} \\ & - 2(1 - \sqrt{2}\,\eta^*) e^{-\sqrt{2}\eta^*} \sin\sqrt{2}\,\eta^* \Big] \end{aligned} \tag{11}$$

in which $\hat{u}_{\infty 2}^* = 3\pi^2/8\sinh^4 h^*$. The approximate solution for u_2^* , which must satisfy the boundary conditions, $u_2^* = 0$ at $\eta^* = 0$ and $u_{2p}^* = u_{\infty 2}^*$, $\partial u_{2s}^*/\partial \eta^* = 0$ as $\eta^* \to \infty$, as shown by Schlichting (Ref. 6) taking into account $u_2^* = u_{2p}^* + u_{2s}^*$ where u_{2p}^* denote the periodic and u_{2s}^* the steady contribution of the second approximation, respectively, is given by:

$$
\begin{aligned}
u_2^* = &- \hat{u}_{\infty 2}^* \cos 2x^* \left\{ \sin 2t^* - e^{-\sqrt{2}\eta^*} \sin(2t^* - \sqrt{2}\eta^*) \right\} \\
&+ \left(\frac{\pi}{2\sinh h^*} \right)^2 \sin 2x^* \sin 2t^* \left\{ e^{-\sqrt{2}\eta^*} \cos\sqrt{2}\eta^* - e^{-\eta^*} \cos \eta^* \right. \\
&\qquad \left. + \sqrt{2}\eta^* e^{-\eta^*} \sin(\eta^* + \pi/4) \right\} \\
&+ \left(\frac{\pi}{2\sinh h^*} \right)^2 \sin 2x^* \cos 2t^* \left\{ - e^{-\sqrt{2}\eta^*} \sin\sqrt{2}\eta^* + e^{-\eta^*} \sin \eta^* \right. \\
&\qquad \left. + \sqrt{2}\eta^* e^{-\eta^*} \cos(\eta^* + \pi/4) \right\} \\
&+ \frac{\pi}{8\sinh^2 h^*} \sin 2x^* \left\{ - 3 + e^{-2\eta^*} + 8e^{-\eta^*} \sin \eta^* + 2e^{-\eta^*} \cos \eta^* \right. \\
&\qquad \left. - 2\sqrt{2}\eta^* \cos(\eta^* + \pi/4) \right\} \qquad \text{...............} \quad (12)
\end{aligned}
$$

Therefore, the approximate solution for the velocity u^* is obtained by substituting Eq.(11) and (12) into Eq.(6). Fig.1-(a) and (b) show the velocity profiles calculated for the case of $\varepsilon = 0.04$ and $\sinh h^* = 1.18$ at $x^* = \pi/2$ and $\pi/4$, respectively, in which $u_{\infty 1} = C\varepsilon\hat{u}_{\infty 1}^* = \pi H/T \sinh kh$. These figures positively demonstrate that at $x^* = \pi/2$, the positive, maximum velocity of a water particle in the boundary layers is identical with the negative one, but that at $x^* = \pi/4$, the positive motion is less than the reverse movement. Seemingly, these results are important, since the direction of sediment movement may be determined by the larger of the two maximum values of the velocity.

Fig. 2 shows the relationship between $u/u_{\infty 1}$ and η^* for the various values of ε ; that is, the effects of convective terms in the boundary layer equations on the velocity profile. This figure indicates that the maximum velocity in non-dimensional form slightly increases with the increasing of the values of ε.

MASS TRANSPORT VELOCITY IN BOUNDARY LAYERS UNDER STANDING WAVES

Longuet-Higgins gives the mass transport velocity in the boundary layers in non-dimensional form, $\bar{U}^*$ as

$$\bar{U}^* = \varepsilon \bar{U}_1^* + \varepsilon^2 \bar{U}_2^* + \cdots\cdots \tag{13}$$

in which $\bar{U}^* = \bar{U}/C$, $\bar{U}_1^* = 0$ and

$$\bar{U}^* = \frac{1}{2\pi} \left\{ \int_0^{2\pi} u_2^* \, dt^* + \overline{\int^{t^*} u_1^* dt^* \frac{\partial u_1^*}{\partial x^*}} + \overline{\int^{t^*} w_1^* dt^* \frac{\partial u_1^*}{\partial z^*}} \right\} \tag{14}$$

Substituting Eqs.(10), (12) and (14) into Eq.(13), the mass transport velocity in the boundary layers developed on the smooth bottom is given by:

$$\bar{U}^* = \frac{1}{8} \left(\frac{\varepsilon\pi}{\sinh h^*} \right)^2 \sin 2x^* \, K(\eta^*) \tag{15}$$

in which

$$K(\eta^*) = - 3 + 8e^{-\eta^*} \sin \eta^* + 3e^{-2\eta^*} \tag{16}$$

This equation can be rewritten in the form:

$$\overline{U} = \frac{\pi^2}{8} \frac{H^2}{LT \sinh kh} \sin 2kx \; K(\eta^*) \tag{17}$$

which is identical with that obtained by Longuet-Higgins.

Fig.3 shows the result calculated of the vertical profile of the mass transport velocity in the boundary layer to the case of standing waves. An outstanding feature which this figure shows is that the transport near the bottom, that is the lower layer, for the range of $\eta^* < 0.9$, is always in the direction from the anti-node to the node of the standing waves, but the transport in the upper layer for the range of $\eta^* > 0.9$ is contrary to the lower one.

In any discussion of bar formation, this result is important, since the direction of sediment movement may be determined by the ratio of sediment diameter d with the boundary layer thickness parameter δ .

EXPERIMENTS ON MASS TRANSPORT VELOCITY IN BOUNDARY LAYERS

EXPERIMENTAL EQUIPMENT - Experimental apparatus consists of a glass side wave tank 3.0 m long, 30 cm wide and 70 cm deep, as shown in Fig.4. The walls are vertical and the glass bed is horizontal. Standing waves were produced by a flutter type wave genarator installed at one end of the tank. Wave heights were measured by an electric resistance type wave gage placed at the anti-node position.

METHODS OF MEASUREMENT - The first method of observing the mass transport velocity involved photographing dye streaks obtained by dropping small grains of potassium permanganate, which sank to the bottom with negligible solution enroute, into water. This method proved advantageous in that a series of water particle displacements could be recorded in a single exposure as shown in Photo. 1, since a conspicuous dye streak was produced in the boundary layer every cycle. The maximum displacement of water particles and its vertical profiles per cycle were measured from similar photographs.

The second method was to examine the transport in the opposite direction near the bottom as predicted by theory. The method involved photographing the movement of vinyl pellets (median diameter 0.13 mm, specific gravity 1.15) which were spread in a thin, uniform layer on the bottom before beginning the tests.

The third method of recording the mass transport velocity involved photographing displacements of a small nylon particle that had the same density as water every 5 cycles of waves using a strobo-scope. When the wave period and water depth are maintained constant, and wave heights are gradually increased, flows in bottom boundary layers undergo a transition from the laminar to the turbulent regime. Therefore, the dye-streak method mentioned above cannot be used because of the dispersion of dye. Then, measurement of the mass transport velocity in the turbulent boundary layers was made using nylon particles (diameter 3 mm). Photo. 2 shows an example of a series of displacement of a nylon particle.

SUMMARY OF EXPERIMENTAL RESULTS - Fig. 5 and 6 show the results of the maximum displacements observed by the dye-streak method for the h/L values of 0.16 and 0.08, respectively. The experiments were carried out by measuring the maximum displacement $\overline{U}_{max}T$ for varying wave heights and for a wave period and water depth that were kept constant. In these figures, the theoretical curve which describes the non-dimensional, maximum displacement of a water particle in the boundary layer, λ^*, can be given by putting $\eta^* = 3.94$ in Eq.(17):

$$\lambda^* = -\sin 2kx \tag{18}$$

in which

$$\lambda^* = \overline{U}_{max}T/(3.12\,\pi^2 H^2/8L\ \sinh^2 kh) \tag{19}$$

and $\overline{U}_{max}$ is the maximum mass transport velocity in the boundary layer. Although the scatter of points can be seen, these figures show that the results of the experiments are in agreement with theory except when the wave height is as small as 4 cm. Russell and Osorio(Ref.7) showed in their experiments in the case of progressive waves, that low waves result in faster transport values than high waves when plotted non-dimensionally. It seems that their results are identical with those of the authors in the case of standing waves.

Fig.7 shows the observed mass transport velocity profiles in the boundary layer for the h/L values of 0.16 and 0.08. It is found that the results are in good agreement with the theoretical curve shown by a full line for the range of $\eta^*>3.0$.

But it was not possible to measure accurately the mass transport velocity in the lower layer for the range of $\eta^* < 0.9$ by this method. Therefore, the different method mentioned above was used to examine the transport in the opposite direction near the bottom as predicted by the theory.

Photos.3 and 4 show the results of the experiments in the h/L value of 0.16 for wave heights 3.3 cm and 8.0 cm, respectively. Both ends of the photographs correspond to the anti-node positions and the center to the node position of the standing waves. In addition, the white and black parts of the photographs show the vinyl pellets and the bottom of the wave tank, respectively. The photographs demonstrate that the transport of the vinyl pellets is in the direction of the node position, and that high waves result in faster transport of vinyl pellets than low waves. Thus, the experimental evidence is in qualitative agreement with the theory.

Fig.8-(a), (b) and (c) show the results of the experiments in h/L = 0.08 for wave heights of 12 cm, 16 cm and 19 cm, respectively. These figures indicate that the experimental values of λ^* are less than those predicted by the theory. Collins (Ref.8) and Brebner (Ref.9) found that in the experiments in the case of progressive waves, the observed mass transport velocity near bottoms is less than that predicted by laminar theory as the bottom boundary layer becomes turbulent. The results for standing waves also indicate that at the inception of turbulence there is a break from the laminar theory in which $\bar{U}_{max}$ is proportional to H^2.

Fig. 9 shows the relationship between $|\bar{U}_{max}|L$ and $H^2(T \sinh^2 kh)^{-1}$ $\times|\sin 2kx|$ for laminar and turbulent ranges. In addition, the limiting value indicated by Brebner and Collins is also shown in this figure. In the case of progressive waves, Brebner and Collins proposed a critical Reynolds number defined by $V_0\delta/\nu$ and obtained the value of 160, in which V_0 is the maximum velocity at the bottom on the basis of the linearized wave theory. Therefore, replacing V_0 by $\pi H(T \sinh^2 kh)^{-1}|\sin 2kx|$ gives the critical Reynolds number in the case of standing waves.

CONCLUSION

The following conclusions may be derived from the results of this study:

1) The mass transport in a laminar boundary layer is in agreement with the theoretical value except for the low waves and the direction of the mass transport in the upper layer is contrary to that of the lower one.

2) In the case of standing waves, boundary layers are turbulent at higher Reynolds number than 160, which is a critical one, and the mass transport is less than the theoretical value for laminar boundary layers.

ACKNOWLEDGEMENTS

The author wishes to express his great appreciation to Prof. Y. Iwagaki for his encouragement in carrying out this study and to Messrs. T. Shibano, Y. Kawashima and A. Kimura for their co-operation in the experiments.

REFERENCES

(1) Lettau, H. (1932). Stehende Wellen als Ursache und Gestaltender Vorgange in Seen; Ann. d. Hydrogr. u. Mar. Met. 60, Jahrg, p. 385.

(2) Nomitsu, R. (1943). Generation of Sand Bar and Sand Ripple due to Stationary Waves: The Geophysics, Vol. 7, No. 1, pp. 61-79. (in Japanese).

(3) Hayami, S. (1950). On the Buried Tomari Harbor: Proc. of JSCE, Vol. 35, No. 4, pp. 167-171. (in Japanese).

(4) Longuet-Higgins, M.S. (1953). Mass Transport in Water Waves: Phil. Trans. Royal Soci., London, Series A. No. 903, pp. 535-581.

(5) Iwagaki, Y. and Tsuchiya, Y. (1966). Laminar Damping of Oscillatory Waves due to Bottom Friction: Proc. 10th Conf. on Coastal Eng.,pp 149-174.

(6) Schlichting, H. (1960). Boundary Layer Theory, translated by J. Kestin:McGraw-Hill, Series in Mechanical Eng., pp. 207-229.

(7) Russell, R.C.H. and Osorio, J.D.C. (1958). An Experimental Investigation of Drift Profiles in a Closed Channel: Proc. 6th Conf. on Coastal Eng., pp. 171-183.

(8) Collins, J.I.(1963). Inception of Turbulence at the Bed under Periodic Gravity Waves: Jour. Geophs. Res., Vol. 68, pp. 6007-6014.

(9) Brebner, A., Askew, J.A. and Law, S.W. (1966). The Effect of Roughness on the Mass-Transport of Progressive Gravity Waves; Proc. 10th Conf. on Coastal Eng., pp. 175-184.

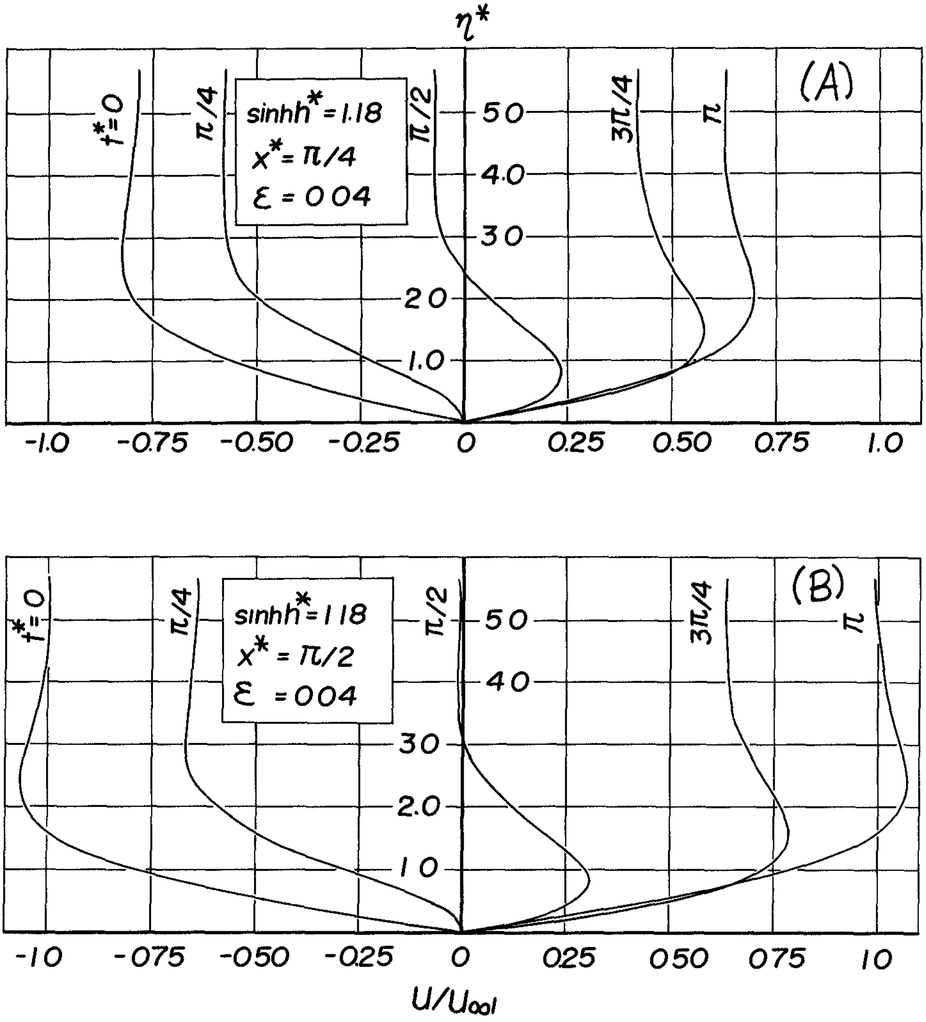

Fig. 1 Velocity profiles in the boundary layer.

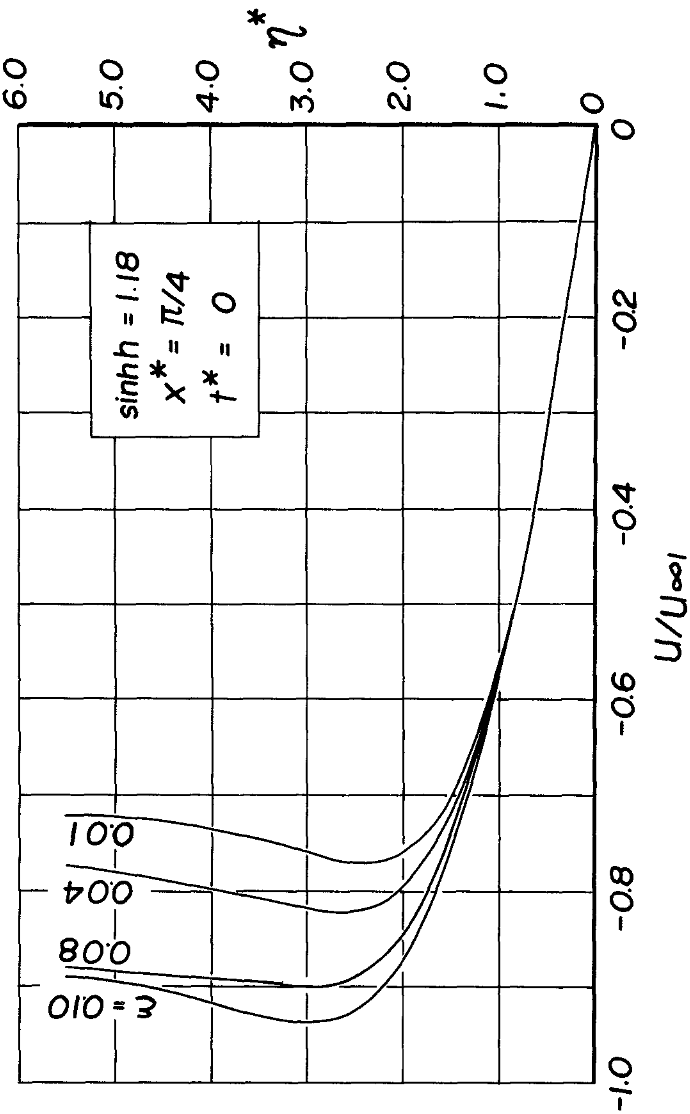

Fig. 2 Effects of H/L value on velocity profile.

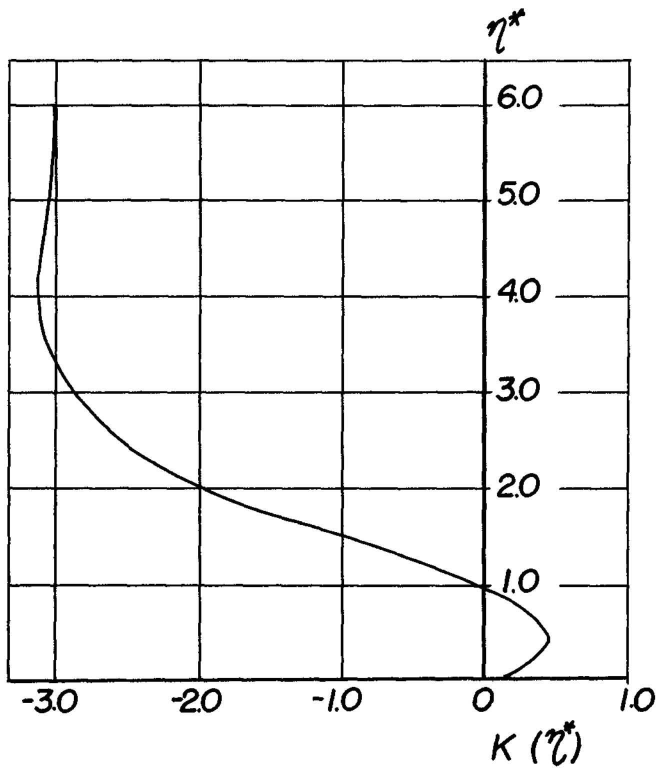

Fig. 3 Distribution of non-dimensional mass transport velocity.

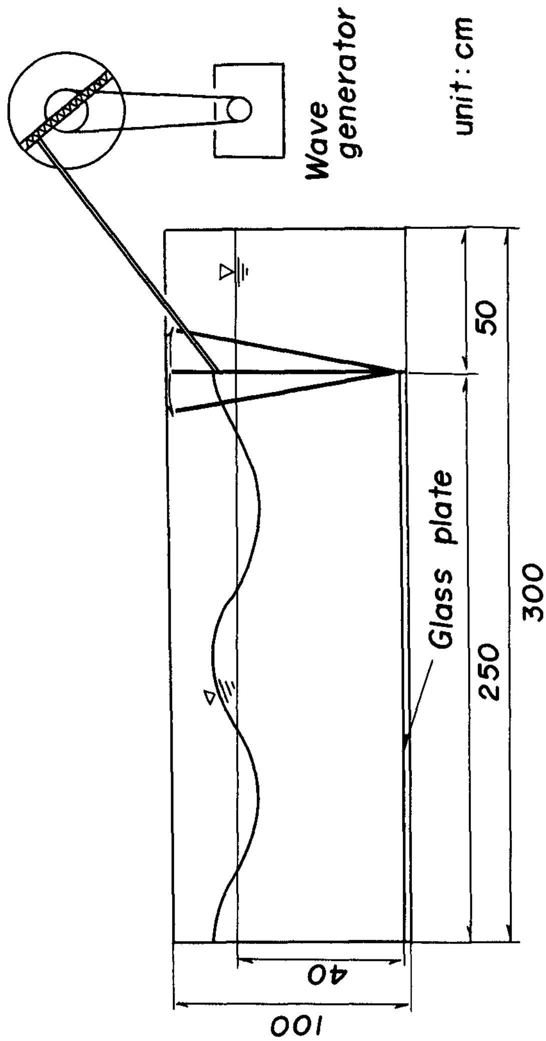

Fig. 4 Schematic view of wave tank.

Photo. 1 An example of dye streaks.

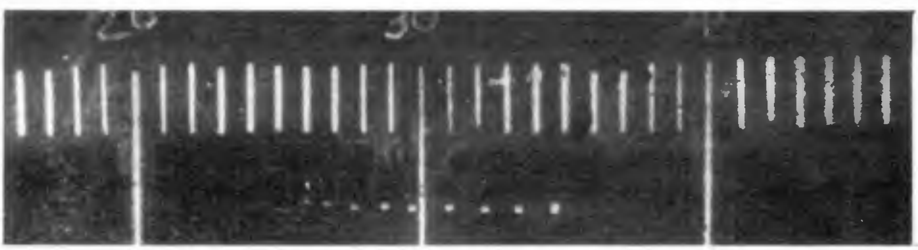

Photo. 2 An example of movement of a nylon particle.

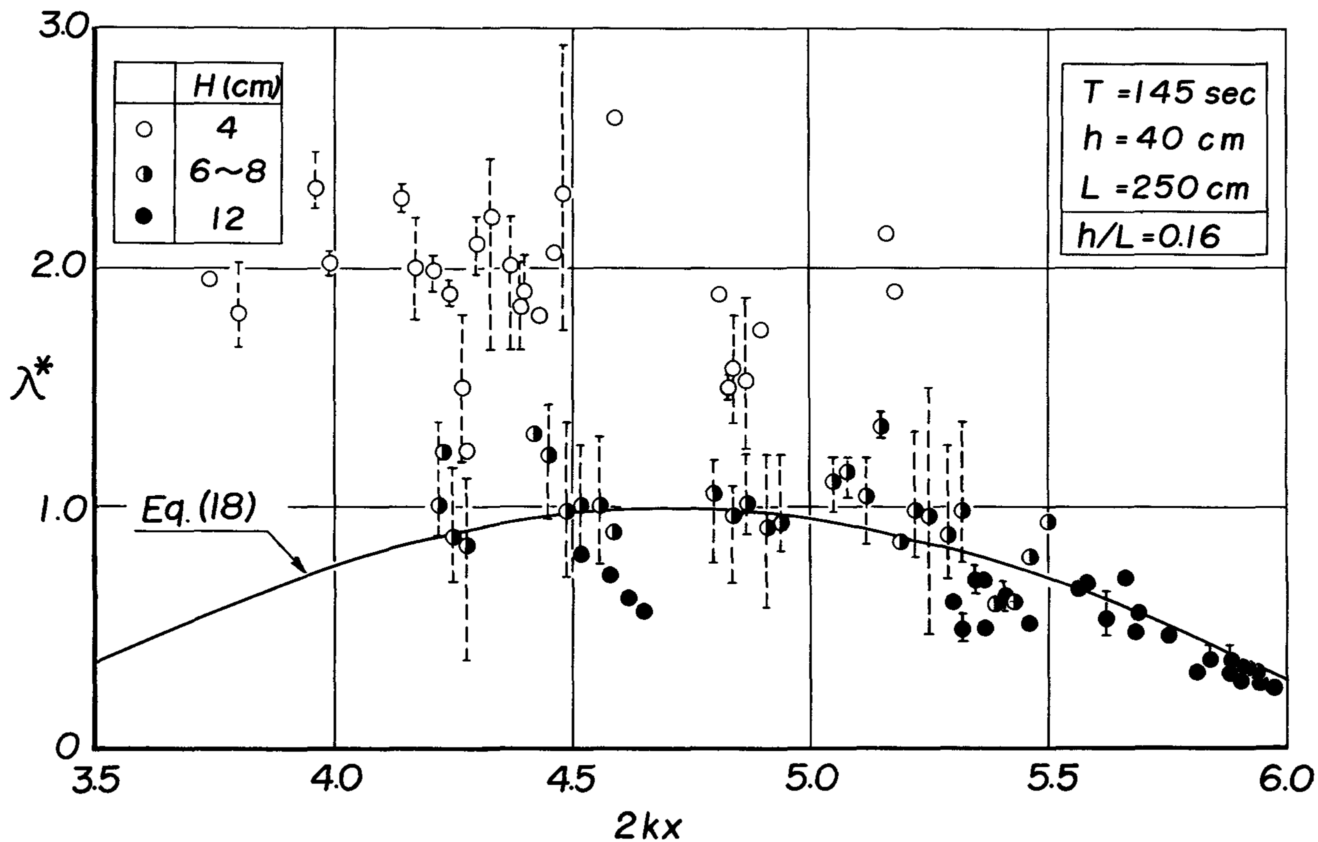

Fig. 5 Comparison between theoretical and experimental non-dimensional mass transport velocity by dye-streak method. (T = 1.45 sec., h/L = 0.16)

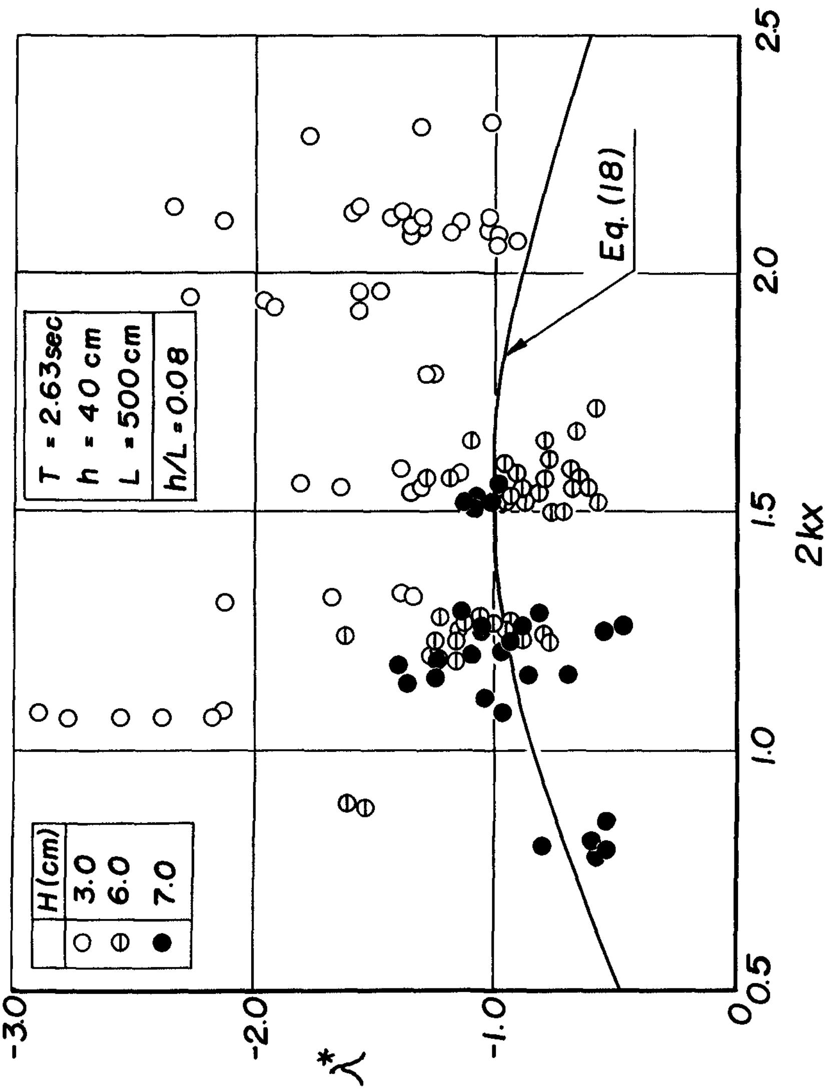

Fig. 6 Like Fig. 5 but (T = 2.63 sec., h/L = 0.08).

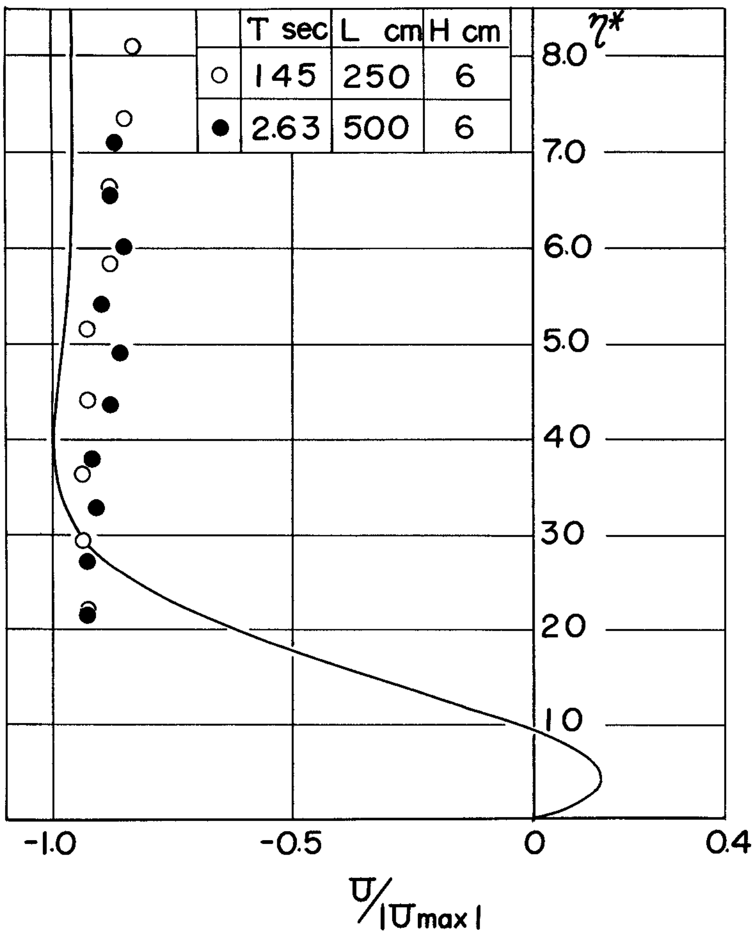

Fig. 7 Comparison between theoretical and experimental non-dimensional mass transport velocity profile.

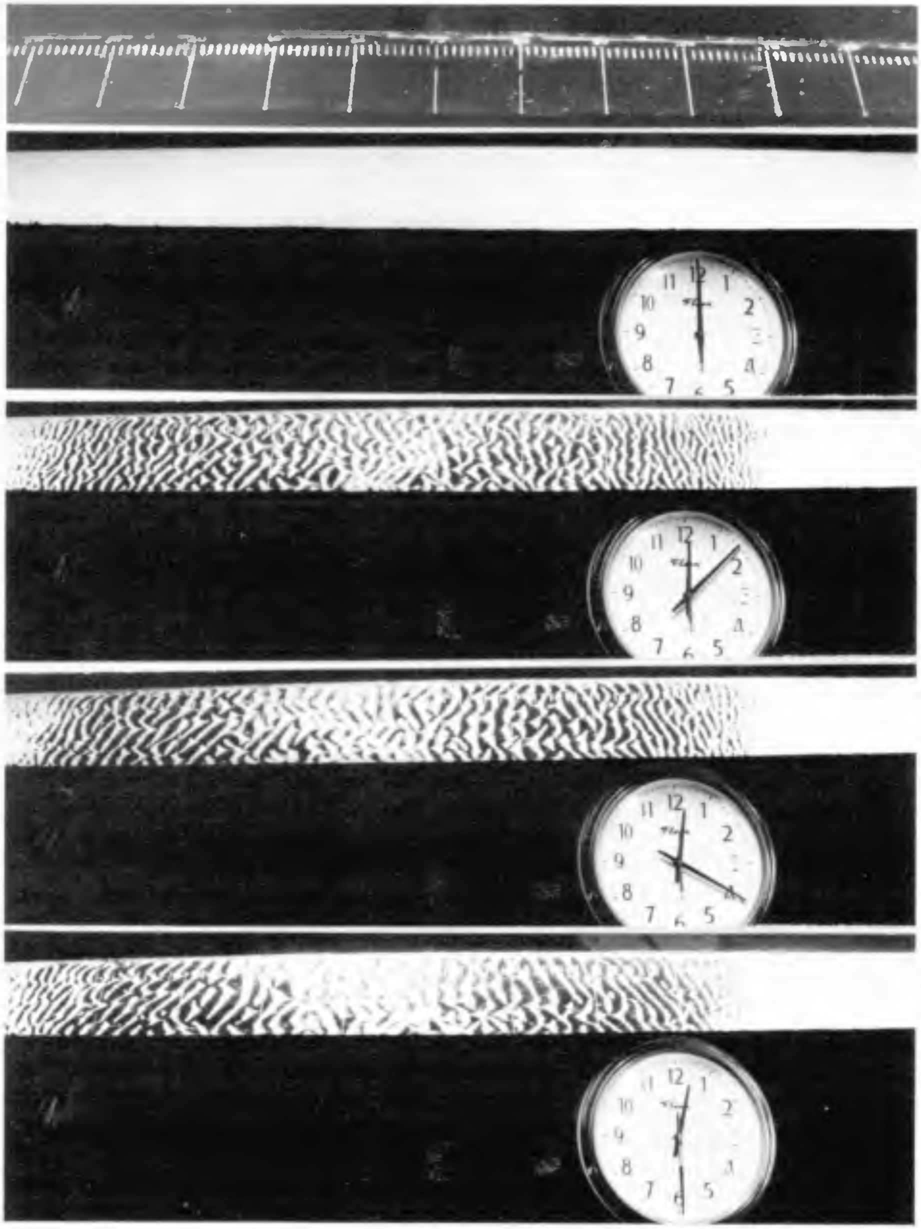

Photo. 3 Movement of vinyl pellets near bottom with time (H = 3.3 cm).

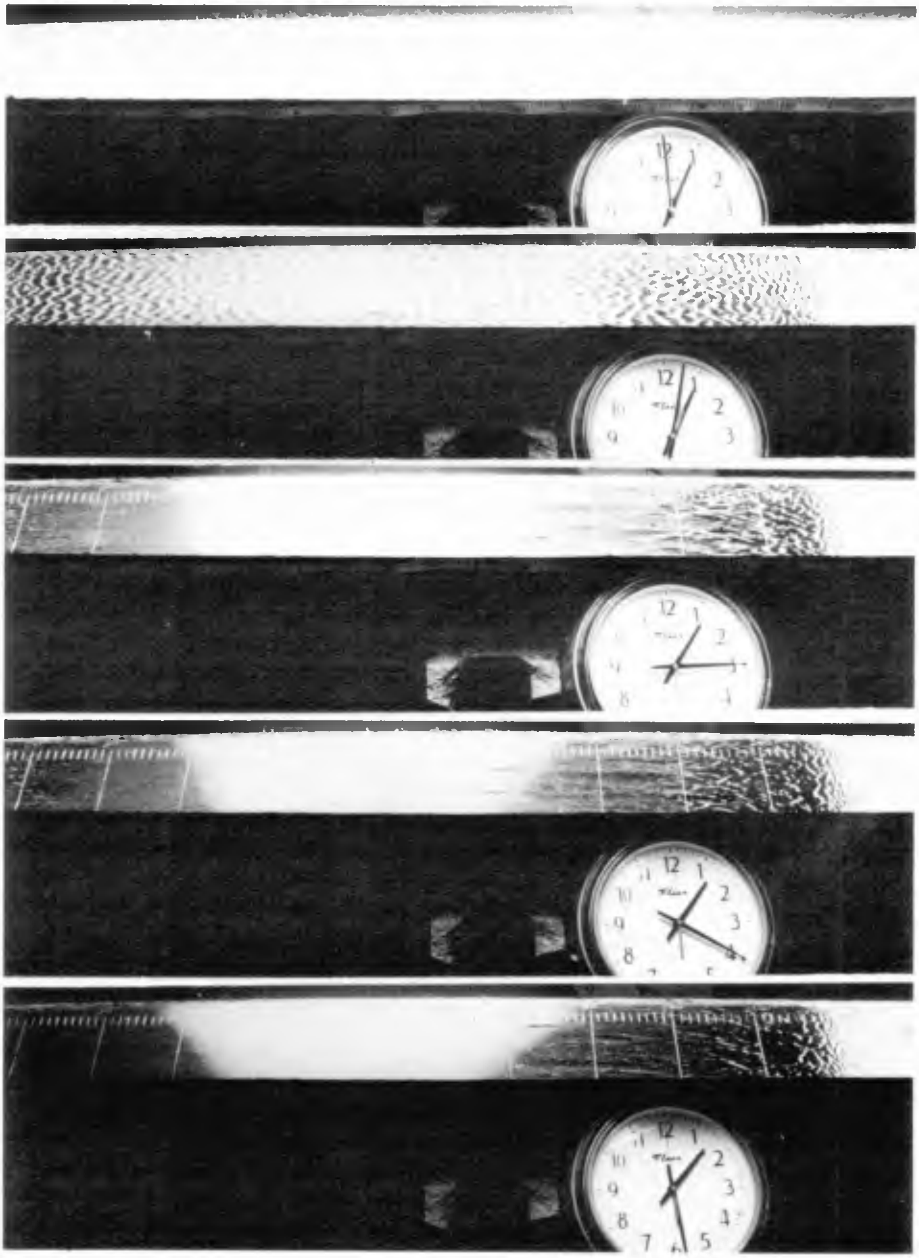

Photo. 4 Movement of vinyl pellets near bottom with time (H = 8.0 cm).

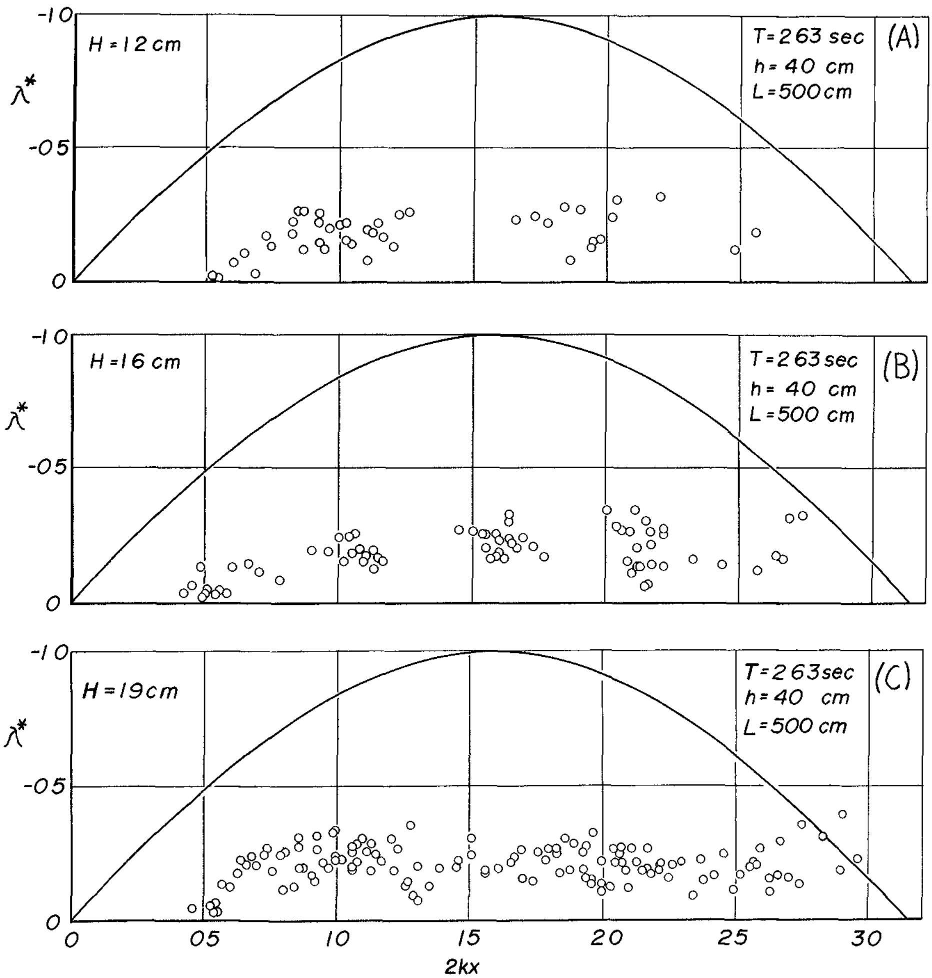

Fig. 8 Comparison between theoretical and experimental non-dimensional mass transport velocity by solid-particle method.

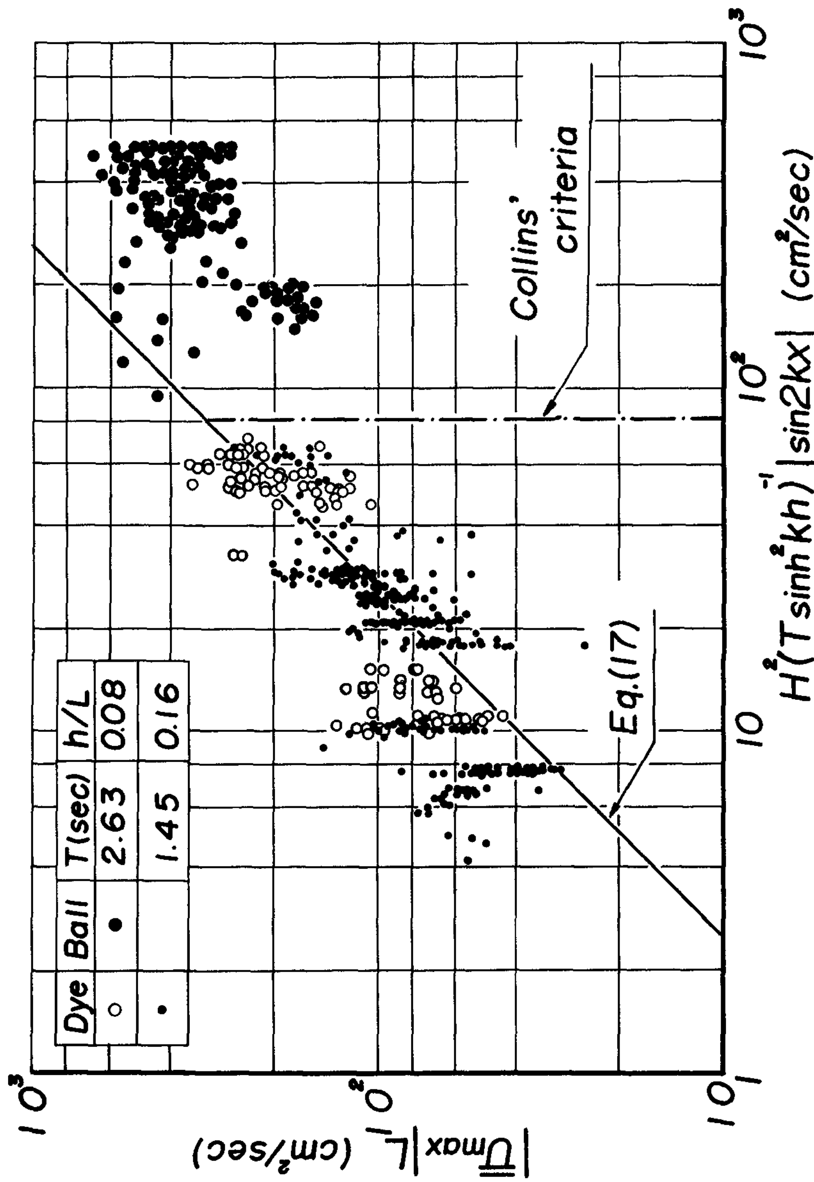

Fig. 9 Relationship between $|\overline{U}_{max}|_L$ and $H^2(T \sinh^2 kh)^{-1} \times |\sin 2kx|$ for the smooth bottom.